Materials Science & Engineering B 226 (2017) 171–176

Contents lists available at ScienceDirect

Materials Science & Engineering B

journal homepage: www.elsevier.com/locate/mseb

Synthesis and characterization of $Dy_3Fe_5O_{12}$ nanoparticles fabricated with the anion resin exchange precipitation method

R. Ivantsov[a,*], N. Evsevskaya[b], S. Saikova[c], E. Linok[b], G. Yurkin[a,c], I. Edelman[a]

[a] Kirensky Institute of Physics, Federal Research Center of Krasnoyarsk Science Centre of Siberian Branch of Russian Academy of Sciences, Krasnoyarsk 660036, Russia
[b] Institute of Chemistry and Chemical Technology, Federal Research Center of Krasnoyarsk Science Centre of Siberian Branch of Russian Academy of Sciences, Krasnoyarsk 660036, Russia
[c] Siberian Federal University, Krasnoyarsk 660041, Russia

ARTICLE INFO

Keywords:
$Dy_3Fe_5O_{12}$ nanoparticles
Anion resin exchange precipitation method
Magnetic circular dichroism

ABSTRACT

Dysprosium-iron garnet (DyIG) nanoparticles were synthesized with the new modification of the anion resin exchange precipitation method. Fourier transform infrared spectroscopy, X-ray diffraction, and transmission electron microscopy showed nanoparticles to be of the garnet structure with an excellent crystallinity. Magnetic properties were studied by using QUANTUM Design MPMS-XL system and the visible magnetic circular dichroism (MCD). Nanoparticles magnetic properties were close to those of bulk DyIG crystals. Dependence of the nanoparticles magnetization (M) on the external magnetic field (H) is described by a narrow hysteresis loop in relatively low fields and the strong linear M increase with the further H increase. The visible MCD of DyIG was studied in this work for the first time. The MCD spectra consisted of several peaks associated with electron transitions in iron and dysprosium ions located in different spectral intervals. Dependences of the MCD peak intensities on temperature and magnetic field were studied.

1. Introduction

Yttrium and rare earth iron garnets ($Y_3Fe_5O_{12}$, $R_3Fe_5O_{12}$, YIG and RIG) have been a source of inexhaustible interest since early 1950's, when Yoder and Keith obtained YIG crystal for the first time [1], and Bertaut and Forret [2], and Geller and Gilleo [3] reported about magnetic properties of YIG and GdIG, respectively. The interest is based on a great variety of garnet physical properties, in particular, on the phenomenon of the sub-lattices magnetic moments compensation which is observed in most of rare earth iron garnets [4]. On the other hand, yttrium and rare earth garnets are widely used as components of microwave devices [5], circulators [6], phase shifters [7], magneto-photonic devices [8], etc. Last decades the YIG and RIG nanocrystals [9–14] gained one of central positions in physics and technology of magnetic materials. Since the properties of nanoscale materials depend on features of the technology, in each case it is necessary to determine in what way properties of nanoparticles correspond to bulk counterparts. That is why it looks being interesting to study separately the temperature behavior of the iron and rare earth sublattices magnetization. As far as we know, this question has not been considered in papers on DyIG nanoparticles yet. The visible magnetic circular dichroism (MCD) – one of the highly informative magneto-optical effects [15], seems to be proper tool for this aim.

The MCD spectral and temperature dependences are helpful for in-depth understanding of the nanoparticles electronic structure and electronic excitations under the influence of an electromagnetic irradiation. This effect is widely used in chemistry of both organic and complex inorganic compounds and in biological studies [16]. Until now, MCD has been rather rarely used to study ferro- and ferrimagnets. The series of works of G.A. Gehring with co-authors reported the MCD study of the manganite, magnetite, ZnO, and doped ZnO thin films [17–19]. Many authors investigated Faraday rotation (FR) in variety of YIG and RIG crystals and films [20–22]. However, FR spectra are less informative comparing to MCD ones. The MCD study was carried out only for $Y_3Fe_5O_{12}$ thin films [23,24] and slices cut from bulk crystals [25], and for $Er_3Fe_5O_{12}$ thin crystal plates [26]. $Dy_3Fe_5O_{12}$ (DyIG) is exceptionally suitable for the MCD investigation. Several narrow f-f bands in Dy^{3+} ions: $^6H_{15/2} \rightarrow {}^6F_{3/2}, \rightarrow {}^6F_{5/2}, \rightarrow {}^6(F_{7/2} + H_{5/2})$ occur in the energy region 11000–14000 cm^{-1}, where electron transitions in Fe^{3+} ions are of extremely low intensities. This range of energy is of high interest for applications because of the possibility to use here new laser sources of radiation. On the other hand, there are no Dy^{3+} f-f bands in the higher energy region where main MCD peaks due to transitions in Fe ions are observed. These circumstances make it

* Corresponding author.
E-mail address: ird@iph.krasn.ru (R. Ivantsov).

http://dx.doi.org/10.1016/j.mseb.2017.09.016
Received 25 May 2017; Received in revised form 5 September 2017; Accepted 21 September 2017
Available online 29 September 2017
0921-5107/ © 2017 Elsevier B.V. All rights reserved.

possible to study separately the temperature and field dependences of MCD of the rare-earth and iron sublattices.

The nanoparticle properties depend strongly, sometimes crucially, on the preparation conditions as it was mentioned above. A fairly complete overview of ferrite nanoparticles fabrication techniques is presented in Ref. [27]. Despite the variety of the used techniques each of them is not universal; therefore, the creation of new techniques or new modifications of the known techniques for obtaining $Dy_3Fe_5O_{12}$ garnet is a problem of high topicality. Some of co-authors of the present paper reported earlier a new way of synthesizing various compound nanoparticles such as α-$Co(OH)_2$, α-$Ni(OH)_2$, $CoAl_2O_4$, $NiAl_2O_4$, Y_3Fe_5O12, $Y_3Al_5O_{12}$, Dy_2O_3, using precipitation method in the presence of the strong base anion exchange resins in OH-form [28–34]. This technique involves anion exchange between the resin and the solution and precipitation of an insoluble compound of metal from the solution. The resin sorbs impurity anions from the reaction solution, while in the case of an ordinary reagent method these impurities and ions which are derived from precipitation reagent, for example, sodium hydroxide or ammonia, remain in the product and complicate the formation of uniform particles. The process of anion resin exchange precipitation is carried out under controlled conditions at constant pH level. More details on the advantages of anion resin exchange precipitation are reported in [35].

As far as we know, the anion resin exchange precipitation method was not used earlier for DyIG nanoparticles preparation. It is worth noting that in this study we use the anion exchange resin in CO_3-form, we suppose that in this case the particles of smaller size and better crystallinity can be produced as compared to the exchange resin in OH-form. The structure, morphology, magnetic and magneto-optic properties of the synthesized nanoparticles are investigated. The study of the MCD spectral and temperature dependences allowed to separate contributions of iron and rare earth sublattices and to analyze their behavior in the region of the magnetic compensation temperature.

2. Experimental

2.1. Synthesis of DyIG nanoparticles

The anion-exchange resin AV-17-8 produced by “Azot” Corporation (Cherkassy, Ukraine) in the chloride form with grain size 0.25–0.5 mm (Russian GOST 20301-74) was transformed into the CO_3 form using its three times treatment with 1 M Na_2CO_3 solution during 1 h, and extensive washing with water to neutral reaction. The total exchange capacity of the anion resin was determined using 0.1 M HCl.

In a typical procedure, mixture of 9.4 ml 0.25 M $Dy(NO_3)_3$ and 15.6 ml 0.25 M $Fe_2(SO_4)_3$ (both chemicals were purchased from JCS “Chemreaktivsnab”, Ufa, Russia) was added drop wise to the 40 ml of anion resin AV-17-8 in CO_3-form under vigorous stirring for 1 h. Molar ratio Dy/Fe was 3:5. After the reaction, the anion resin beads were removed using a sieve, the precipitate was centrifuged, washed with distilled water several times and finally dried in air at 100 °C to form a precursor. Subsequently, precursor was calcined at 850 °C for 2 and 5 h in order to produce $Dy_3Fe_5O_{12}$.

2.2. Nanoparticles characterization

Powder X-ray diffraction was carried out using PANalytical X'pert Pro diffractometer equipped with a Cu Kα anode. Fourier transformed infrared spectra (FT-IR) were recorded on a Bruker Vector 22 spectrometer. Transmission electron microscope (TEM), Hitachi H-800, was used to characterize the morphology and microstructure of the samples.

Magnetization hysteresis loops were recorded with a QUANTUM Design MPMS-XL system at temperature 298 K with magnetic field value up to 50 kOe.

Transparent samples containing the nanoparticles were prepared for magnetooptical measurements: the nanoparticles powder was mixed with dielectric transparent silicon-based glue “Rayher” art. nr. 3338100 (purchased from “Digl Design” Co.- official distributer of the Rayher Co., Germany) in the weight proportion 0.5/100 and measures were undertaken to obtain the homogeneous particles distribution in a matrix such as ultrasonic bath. The low magnetic powder concentration allowed us to exclude the interaction between nanoparticles. The mixture was placed between two thin glass plates spaced by wires 0.15 mm in diameter and solidified.

MCD was measured with the laboratory made installation. The plates were placed between poles of electromagnet with the drilled cylindrical holes through which the light beam passed. Thus directions of the light beam and the magnetic field were parallel to each other and perpendicular to the plane of the plate. The light wave polarization state was modulated from the right-hand to the left-hand circular polarization relatively to the magnetic field direction. The modulator was made of a fused optical isotropic silica prism with a glued piezoelectric ceramic element. Application of ac voltage results in excitation of a standing elastic wave in the prism if the voltage frequency ω coincides with the prism eigen frequency (28.6 kHz in our case). As a result, the prism becomes optically anisotropic: the axis oriented perpendicular to the direction of light propagation becomes a fast optical axis on the compression wave and slow one on the stretching wave. Light wave linearly polarized at an angle of 45° relatively to the optical axis of the prism turns into the circularly polarized wave at the exit from the prism: right-hand relative to the light propagation vector in the half-cycle of compression and left-hand in the half-period of stretching. The light absorption in the sample with MCD will be different for these two polarizations, and so the light flux after passing through the sample will be modulated in intensity. Accordingly, the signal at the output of the photomultiplier will also be modulated. The difference between the photomultiplier signals for two opposite directions of an applied magnetic field was equal to MCD value multiplied by 2. Measurements were carried out in the spectral range $(10–26)\cdot10^3$ cm^{-1} in a magnetic field of up to 1.2 T at 300 K and up to 0.5 T for lower temperatures. The measurement accuracy was about 10^{-4}, and the spectral resolution was 20–50 cm^{-1} depending on the wavelength.

3. Results and discussion

3.1. Nanoparticles structure, phase, and morphology

As is known, to obtain pure crystals of ferrite garnet with reproducible properties, it is necessary to provide the stoichiometric ratio of cations, Dy:Fe = 3:5, and the complete precipitation of that to be achieved. Process for the obtaining precursor can be represented as follows:

$$24RX + 3\ DyA_3 + 5\ FeA_3 \rightarrow 24RA + \{3\ Dy\ X_3 + 5\ FeX_3\},$$

RX, RA are the anion-exchange resins (X = $1/2CO_3^{2-}$; A = $1/2SO_4^{2-}$, NO_3^-).

In our case, the precipitation of cations from the solution occurred completely, since the residual concentration of metals in the solution was less than 1% according to the atomic absorption analysis.

The FT-IR spectrum of product synthesized at the precursor calcination temperature 850 °C is presented in Fig. 1. The major band in the range of 560–670 cm^{-1} consists of three frequency bands: ν_1 at 652 cm^{-1} is caused by the stretching vibrations of the tetrahedral iron-oxygen bonds, ν_2 at 601 cm^{-1} is caused by the iron -oxygen vibration in octahedral sites, and ν_3 at 564 cm^{-1} is due to the dodecahedral dysprosium-oxygen bonds. These bands coincide totally with bands observed in the FT-IR spectrum of DyIG nanoparticles synthesized with glycine assisted combustion method [36]. Thus, the spectrum can be considered as an evidence of the formation of the garnet nanoparticles.

XRD patterns of the powder samples synthesized shown in Fig. 2 contain all peaks characteristic for $Dy_3Fe_5O_{12}$: the peak positions and their intensities ratio correspond to the ICDD card number 73–1378 for this compound. No peaks evidencing on other crystal phases are

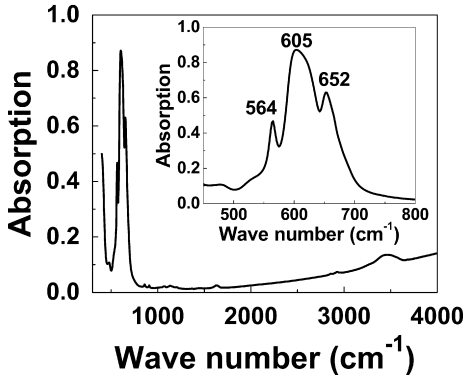

Fig. 1. FT-IR spectrum of DyIG nanoparticles at energies 500–4000 cm^{-1}. Inset: enlarged region of 500–800 cm^{-1}.

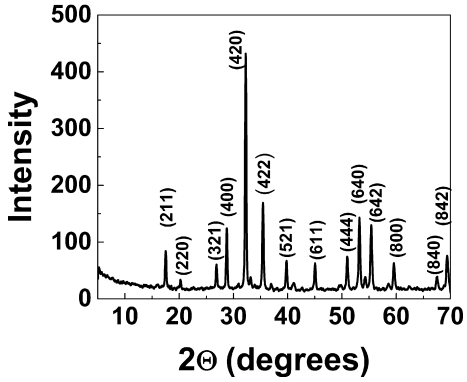

Fig. 2. X-ray diffraction pattern of DyIG nanoparticles.

detected. So, the product contains $Dy_3Fe_5O_{12}$ nanocrystalline particles. The mean size of nanocrystallites was estimated with the Scherrer method [37] using the full-width half maximum of the diffraction peak (4 2 0). It appeared to be of about 15.2 nm. The calcination temperature is known to be one of the main factors affecting in the formation of the garnet phase, and it is worth noting that in our case the calcination temperature is lower than that reported in similar works [38]. It is probably concerned with the fact that the method based on anion exchange co-precipitation decreases the temperature of the DyIG formation. Additionally, the use of hydroxides instead of oxides also decreases the temperature due to the higher reactivity of hydroxides in comparison with that of oxides.

The spherical shaped crystalline nanoparticles with distinct atomic planes are clearly seen in the HRTEM image of as-prepared powder sample (Fig. 3a). The particles size is of approximately 20–30 nm which is a little higher comparing to the XRD data. This difference can be due to the fact that the electron microscope gives image of the whole particles while X-ray diffraction detects only their crystallography ordered parts. The crystalline particles are combined in aggregates with a size of about 100 nm as shown in Fig. 3b. The formation of aggregates is due to the strong tendency of nanoparticles to minimize their surface energy.

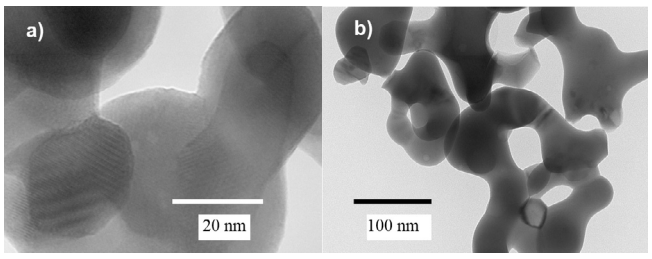

Fig. 3. TEM images of nanoparticles with different magnification.

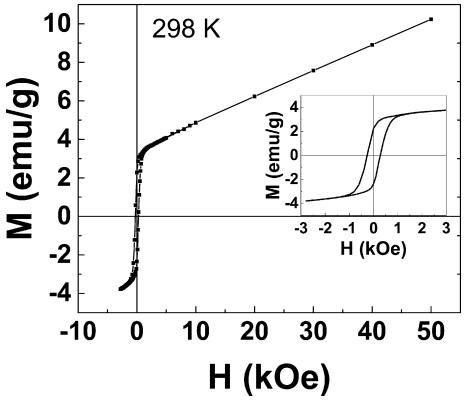

Fig. 4. Magnetization field dependence of DyIG nanoparticles at temperature 298 K. Inset: The hysteresis loop in lower fields.

Similar picture was observed in Ref. [15] for the $Dy_3Fe_5O_{12}$ nanoparticles fabricated with the ball milling technique in a controlled atmosphere; the nanoparticles surface morphology revealed large, rounded formations up to micron sizes, at the same time X-rays detected nanocrystallites with an average size of a few dozens of nanometers (see, Fig. 1b in [15]).

3.2. Nanoparticles magnetization field dependence

The nanoparticles magnetization dependence on an external magnetic field recorded at T = 298 K is presented in Fig. 4. Close to the rectangular shape hysteresis loop with coercivity H_c = 280 Oe is observed which collapses in the field ~1 kOe. At higher fields magnetization increases, practically linear with H. Comparing of the hysteresis loop shape and the magnetization value seems to be reasonable with the data presented in Refs. [37,39] for the DyIG nanoparticles prepared by hydrothermal method and aqueous sol-gel method, correspondingly, using the different samples annealing temperature. For instance, for the annealing temperature 900 °C, H_c was 274 Oe and the magnetization value in magnetic field 4.4 kOe was 4.4 emu/g (Table 4 in Ref. [38]). For nanoparticles synthesized with the hydrothermal method [37], H_c was 928 Oe and magnetization value was of about 4 emu/g in magnetic field of 5 kOe.

Magnetic saturation is not reached up to the maximal field used of 50 kOe. Such a dependence N(H) is characteristic of some of the rare earth iron garnets (gadolinium, terbium, dysprosium, and holmium) For DyIG, the magnetization increase linear in the magnetic field was observed in many works both for nanoparticles and for bulk crystals up to very high H values [37,38,40]. This phenomenon is associated with the competition of the negative exchange interaction between the rare-earth and iron sublattices and the applied magnetic field resulting in an appearance of the non-collinear magnetic structure over a certain interval of magnetic fields ($H_1 < H < H_2$). The field-induced non-collinear magnetic structures in RIG were predicted theoretically [41,42] and revealed experimentally at the end of 1960-s (e.g., [40,43,44], and is still the subject of the intensive research (e.g., [45]). Thus, the magnetization behavior in the high magnetic field observed for the DyIG nanoparticles synthesized is typical for the rare earth iron garnets.

3.3. Magnetic circular dichroism

As it was mentioned in the introduction, magnetic structure of a number of rare-earth garnets undergoes strong changes at the temperature of magnetic compensation. Therefore, it was necessary to follow the temperature dependences of the properties of the investigated nanoparticles in order to evaluate their compliance with the bulk and thin-film DyIG samples. For DyIG bulk crystal T_{comp} = (220 ± 2) K [46], for thin film T_{comp} = 225 K [21]. At temperatures

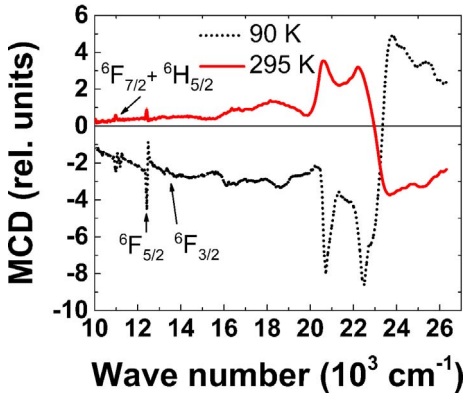

Fig. 5. MCD spectra of composite sample containing DyIG nanoparticles at temperatures 90 (full circles) and 297 (empty circles) K. H = 3.5 kOe.

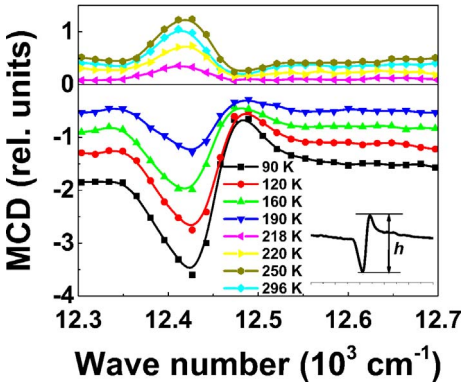

Fig. 6. MCD maximum associated with the transition $^6H_{15/2} \rightarrow {}^6F_{5/2}$ of Dy^{3+} ion at different temperatures. H = 3 kOe. $T_{comp} \approx 215$ K.

higher than T_{comp}, the total sample magnetization should be determined by the iron sublattice, while at $T < T_{comp}$ the total magnetization will be determined by the Dy sublattice magnetic moment directed oppositely relative to the Fe sublattice magnetic moment. That is why the total magnetization becomes equal to zero at $T = T_{comp}$. As MCD is linear function of magnetization, this reordering transition should be reflected in temperature behavior of MCD too. Contrary to the commonly used magnetization measurements, advantage of the MCD technique is possibility to single out contribution from various magnetic sub-lattices.

MCD spectra of the composite sample containing DyIG nanoparticles recorded at two temperatures – significantly above and below T_{comp} of DyIG bulk samples presented in literature, are shown in Fig. 5. First of all, the different sign of the MCD signal is seen at higher and lower temperature what evidences on the reorientation of the sample total magnetic moment, that is, on the magnetic compensation phenomenon in the sample. The picture is similar to that observed in Ref. [26] where MCD spectra of the $Er_3Fe_5O_{12}$ single crystal in the region of the electron transition between the ground state and the first excited state multiplets was studied in dependence on temperature. For convenience of the MCD spectra analysis, it is possible to divide them into two groups of extrema prevailing in different wave length intervals. MCD spectrum in the area of $(18–26)\cdot10^3$ cm^{-1} corresponds almost completely with the MCD spectrum presented earlier [32] for YIG nanoparticles fabricated with the same technique as well with the MCD spectrum of the YIG thin films and thin crystal plates available in literature [23–25,47]. As YIG contain no RE elements, all MCD features in this region can be associated with electron transitions in Fe^{3+} ions both single-ion and charge-transfer type. Note some differences in the identification of the MCD maxima with certain types of electron transitions in the works of different authors. That is why we do not indicate here the names of transitions in this region. Transitions associated with the Fe^{3+} ion occur also in the lower energy spectral region, in particular, features near 10920 and 14090 cm^{-1} due to the transitions $^6A_{1g}(^6S) \rightarrow {}^4T_{1g}(^4G)$ and $^6A_{1g}(^6S) \rightarrow {}^4T_{2g}(^4G)$ were observed in the $Y_3Fe_5O_{12}$ MCD spectrum in Ref. [25]. In Fig. 5, two fairly weak lines are observed at room temperature near the light wave energies 13300 and 10990 cm^{-1}, and one most intensive line centered near 12380 cm^{-1}. These energy values are characteristic for the Dy^{3+} ion transitions from the ground state multiplet $^6H_{15/2}$ to the exited state multiplets $^6F_{3/2}$, $^6F_{7/2}$ + $^6H_{5/2}$, and $^6F_{5/2}$ [48], correspondingly. Evidently, the last one originates from the transition in the Dy^{3+} ion only, while two firsts can overlap partly with the transitions in Fe^{3+} ions. Therefore, its temperature behavior will be used to monitor the Dy sublattice temperature behavior. Since transitions in Dy^{3+} ion occur between deeper levels they are least subjected to an influence of the ion environment, and MCD maxima should be rather narrower comparing to the broad maxima observed at higher energies and due to the transitions in Fe^{3+} ion that is actually observed.

The section of the MCD spectrum near 12420 cm^{-1} is shown in Fig. 6 in dependence on temperature. As the sample is cooled, the MCD decreases, passes through zero, and after change sign its absolute value increases again. Similar temperature behavior observed for all other MCD peaks originated both from Fe^{3+} and Dy^{3+} ion transitions. In Fig. 7, temperature behavior of two MCD peaks associated with Fe and Dy sublattices is shown. The temperature corresponding to zero MCD value, that is, the compensation temperature T_{comp} is the same for both sub-lattices and equals to 214 K. Below T_{comp} the curves in Fig. 7 are completely identical while at temperatures higher than T_{comp} curves for Fe and Dy sublattices differ from each other in some extent. One can indicate that below T_{comp} the Fe and Dy magnetic sublattices are rigidly coupled.

Thus, the temperature changes of the MCD correspond, in principle, to the temperature changes of the magnetization in RIG observed in the works cited above. As concerns magneto-optical effects, similar temperature changes of Faraday rotation (FR) was observed in DyIG films for several wave length [21]. For the film, T_{comp} was 225 K, and the shapes of the curves FR(T) coincided with each other both above and lower 225 K. Some difference between our and Ref. [21] data can be associated with that FR of the film is strongly influenced by the overlapping dispersive shape contributions attributed to Fe^{3+} transitions while MCD maxima of dissipative form allow to separate the contributions of individual sub-lattices for the DyIG and trace their temperature dependences.

Magnetic field dependences of MCD originated from electron transitions in Fe^{3+} (at energy 20200 cm^{-1}) and Dy^{3+} (at energy 12420 cm^{-1}) ions are presented in Fig. 8 for T = 300 K. For both cases, the narrow almost rectangular hysteresis loops are observed with the field of the magnetization saturation of about 2.25 and 3.8 kOe for Fe and Dy sub-lattices, correspondingly. The coercivity H_c values are of

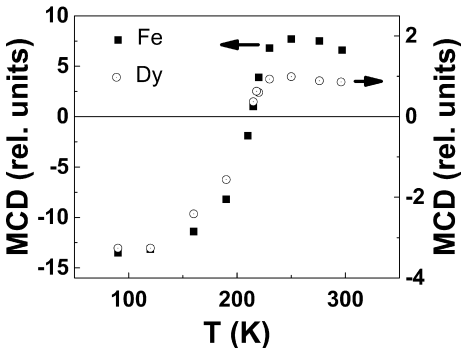

Fig. 7. Temperature dependencies of the MCD intensity in the Fe^{3+} transitions region (area under the curve in the energy interval 20660–22200 cm^{-1}) and in the Dy^{3+} transition (the distance between two extrema, as it is shown in Inset in Fig. 6). H = 3 kOe.

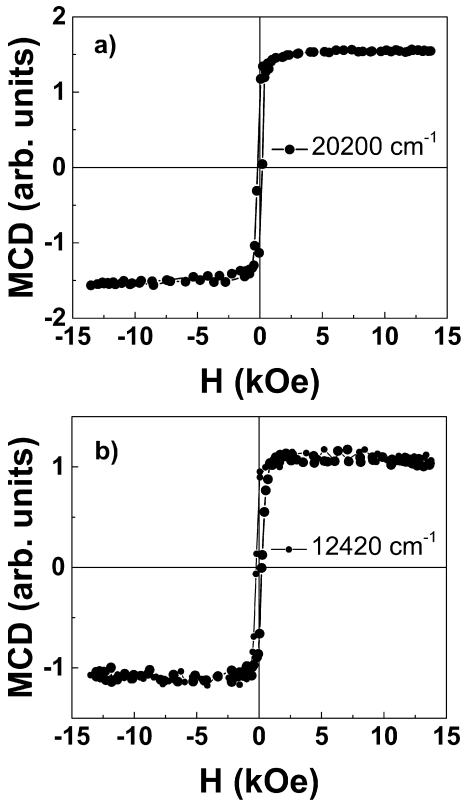

Fig. 8. MCD hysteresis loops for (a) 20200 cm^{-1} (Fe sublattice) and (b) 12420 cm^{-1} (Dy sublattice) at the 297 K.

about 200 Oe. With the sample cooling up to 90 K, the H_C practically does not change. Thus, the coercivity, its temperature dependence, and the hysteresis loop shape obtained from two types of measurements technique – MCD and magnetic measurements – are close with each other. However, MCD and magnetization behavior in the higher magnetic field are quite different (compare Figs. 3 and 8). Similar difference between magnetization and magneto-optical effect (Faraday rotation, FR) is known from the current literature. Authors of Ref. [49] studying the TbIG single crystal, have shown the FR value to be almost independent on magnetic field up to 100 kOe at room temperature. At the same time the TbIG magnetization increases strongly in high magnetic fields [45]. Such a discrepancy is understandable in principle since magneto-optical effects (MCD and FR) are related to the individual sublattices magnetic moments rather than to the total sample magnetization. So, the process of the alignment of the canted magnetic moments of the Fe and RE sublattices effects insignificant in the MCD and RF in high magnetic fields. However, this phenomenon needs further thorough investigation. The set of the results on MCD in YIG nanoparticles obtained here allows undertaking successful work in this direction.

4. Conclusions

DyIG nanoparticles were synthesized with the modified anion resin exchange precipitation method using resin in CO_3-form what provides to produce particles of smaller size as compared to usually used resin in OH-form. The nanoparticles synthesized were of the garnet structure with an excellent crystallinity. No other phases were revealed. The nanoparticles magnetization dependence on an external magnetic field as well as the magnetic field and temperature dependencies of MCD indicate that the magnetic properties of synthesized nanoparticles correspond completely to the properties of the bulk DyIG crystals with all peculiarities inherent in this material including magnetic sub-lattices compensation and strong magnetization increase in high magnetic fields. The contribution of rare-earth Dy ions to the MCD spectrum of DyIG was studied here for the first time. This result can be used for more rigorous studying properties of rare-earth garnets in the region of the magnetic compensation temperature.

Acknowledgement

The work was supported partly by the Grant of the President of the Russian Federation – Russia no. NSh-7559.2016.2, and by the Russian Foundation for Basic Research – Russia (RFBR): grant. No. 16-33-00043.

References

[1] H.S. Yonder, M.L. Keith, Am. Miner. 36 (1951) 519–533.
[2] F. Bertaut, F. Forret, Compt. Rend. 242 (1956) 382–383.
[3] S. Geller, M.A. Gilleo, Acta Cryst. 10 (1957) 239–240.
[4] F. Bertaut, R. Pauthenet, Proc. IEEE 104 B (1957) 261–264.
[5] K. Sadhana, S.R. Murthy, K. Praveena, Mater. Sci. Semicond. Process. 34 (2015) 305–311.
[6] T. Ramesh, R.S. Shinde, S.R. Murthy, J. Magn. Mag. Mater. 324 (2012) 3668–3673.
[7] G.M. Yang, J. Wu, J. Lou, M. Liu, N.X. Sun, IEEE Trans. Magn. 49 (2013) 5063–5068.
[8] A.R. Prokopov, P.M. Vetoshko, A.G. Shumilov, A.N. Shaposhnikov, A.N. Kuzmichev, N.N. Koshlyakova, V.N. Berzhansky, A.K. Zvezdin, V.I. Belotelov, J. Alloys Comp. 671 (2016) 403–407.
[9] V.K. Sankaranarayanant, N.S. Gajbhiye, J. Phys, Condens. Matter 4 (1992) 4857–4870.
[10] M.A. Ahmed, S.T. Bishay, S.I. Eldek, Mater. Chem. Phys. 126 (2011) 780–785.
[11] Z. Cheng, H. Yang, Y. Cui, L. Yu, X. Zhao, S. Feng, J. Magn. Magn. Mater. 308 (2007) 5–9.
[12] H. Xu, H. Yang, W. Xu, L. Yu, Curr. Appl. Phys. 8 (2008) 1–5.
[13] R. Pena-Garcia, A. Delgado, Y. Guerra, B.V.M. Farias, D. Martinez, E. Skovroinski, A. Galembeck, E. Padrón-Hernández, Phys. Stat. Sol. A 213 (2016) 2485–2491.
[14] M. Guillot, C.N. Chinnasamy, J.M. Greneche, V.G. Harris, J. Appl. Phys. 111 (2012) 07A517-07A517-3.
[15] P.J. Stephens, J. Chem. Phys. 52 (1970) 3489–3516.
[16] R. Kripal, M.J. Bajpai, Alloys Comp. 490 (2010) 5–10.
[17] G.A. Gehring, M.S. Alshammari, D.S. Score, J.R. Neal, A. Mokhtari, A.M. Fox, J. Magn. Magn. Mater. 324 (2012) 3422–3426.
[18] M. Ying, W. Dizayee, Z.X. Mei, X.L. Du, A.M. Fox, G.A. Gehring, J. Phys. D 48 (2015) 255502–255510.
[19] T.K. Nath, J.R. Neal, G.A. Gehring, J. Appl. Phys. 105 (2009) 07D709-1–07D709-3.
[20] H. Umezawa, Y. Yokoyama, N. Koshizuka, J. Appl. Phys. 63 (1988) 3113–3115.
[21] J. Ostoréro, M. Escorne, A. Pecheron-Guegan, F. Soulette, H. Le Gall, J. Appl. Phys. 75 (1994) 6103–6105.
[22] M. Guillot, H. Le Gall, J. Gouzerh, J.M. Desvignes, M. Artinian, J. Appl. Phys. 79 (1996) 5932–5934.
[23] J.C. Canit, J. Badoz, B. Briat, R. Krishnan, Solid State Commun. 15 (1974) 767–770.
[24] S. Visnovsky, J.C. Canit, B. BriaT, R. Krishnan, J. Phys. 40 (1979) 73–77.
[25] G.B. Scott, D.E. Lacklison, H.I. Ralph, J.L. Page, Phys. Rev. B 12 (1975) 2562–2571.
[26] P.G. Feldmann, H. Le Gall, M. Guillot, IEEE Trans Magn. MAG-21 (1985) 1669–1671.
[27] K.K. Kefeni, T.A.M. Msagati, B.B. Mamba, Mater. Sci. Eng. B 215 (2017) 37–55.
[28] S.V. Saikova, M.V. Panteleeva, G.L. Pashkov, R.B. Nikolaeva, Zh. Prikl. Khim. (2002) 1823–1826 (in Russian).
[29] G.L. Pashkov, S.V. Saikova, M.V. Panteleeva, E.V. Linok, Theor. Found. Chem. Eng. 48 (2014) 671–676.
[30] G.L. Pashkov, S.V. Saikova, M.V. Panteleeva, E.V. Linok, A.S. Samoilo, G.N. Bondarenko, Glass Ceram. 70 (2013) 225–228.
[31] G.L. Pashkov, S.V. Saikova, M.V. Panteleeva, E.V. Linok, I.V. Korol'kova, Glass Ceram. 71 (2014) 57–59.
[32] G.L. Pashkov, S.V. Saikova, M.V. Panteleeva, E.V. Linok, P.D. Ivantsov, A.M. Zhizhaev, Izv. Vyssh. Uchebn. Zaved. Khim. Khim. Tekhnol. 5 (6) (2013) 77–81 (in Russian).
[33] G.L. Pashkov, S.V. Saikova, M.V. Panteleeva, E.V. Linok, N.P. Evsevskaya, G.N. Bondarenko, A.M. Zhizhaev, L.S. Tarasova, Glass Ceram. 73 (2016) 107–110.
[34] G.L. Pashkov, N.P. Evsevskaya, E.V. Linok, M.V. Panteleeva, G.N. Bondarenko, J. Siber Federal Univ. Chem. 9 (2016) 371–376.
[35] G.L. Pashkov, S.V. Saikova, M.V. Panteleeva, Theor. Found. Chem. Eng. 50 (2016) 575–581.
[36] R. Tholkappiyan, K. Vishista, Appl. Surf. Sci. 351 (2015) 1016–1024.
[37] B.D. Cullity, S.R. Stock, Elements of X-Ray Diffraction, third ed., Prentice-Hall Inc, 2001.
[38] G. Rekha, R. Tholkappiyan, K. Vishista, F. Hamed, Appl. Surf. Sci. 385 (2016) 171–181.
[39] O. Opuchovic, A. Kareiva, K. Mazeika, D. Baltrunas, J. Magn. Magn. Mater. 422 (2017) 425–433.
[40] M. Lahoubi, A. Bouguerra, A. Kihal, G. Fillion, J. Alloys Comp. 275–277 (1998) 598–601.

[41] S.V. Tyablikov, Metody kvantovo1 teorii magnetizma (Methods of the Quantum Theory of Magnetism), Nauka, 1965.
[42] A. Clark, E. Callen, J. Appl. Phys. 39 (1968) 5972–5982.
[43] K.P. Belov, E.V. Talalaeva, L.A. Chernikova, R.Z. Levitin, T.V. Kudryavtseva, S. Amadezi, V.I. Ivanovski1, Zh. Eksp. Teor. Fiz. 58 (1970) 1923; Soviet Phys.-JETP 31 (1970) 1035–1037.
[44] J. Schelling, A. Clark, Phys. Lett. 29A (1969) 172–173.
[45] M. Lahoubi, W. Wang, J. Magn. Magn. Mater. 393 (2015) 437–441.
[46] F. Bertaut, R. Pauthenet, Proc. IEE 104 B (1957) 261–264.
[47] J.C. Canit, R. Krishnan, B. Briat, Sol. State Commun. 42 (1982) 653–657.
[48] P. Gorlich, H. Karras, G. Kotitz, R. Lehmann, Phys. Stat. Sol. 5 (1964) 437–461.
[49] F.M. Yang, N. Miura, G. Kido, S. Chikazumi, J. Phys. Soc. Jpn. 48 (1980) 71–76.